AD-A080 053 DEFENCE RESEARCH ESTABLISHMENT VALCARTIER (QUEBEC) F/G 20/6
EXPERIMENTAL STUDY OF AN OPTICAL GUIDED-BEAM SPLITTER,(U)
OCT 79 D VINCENT, J W LIT, P LAVIGNE, G OTIS
UNCLASSIFIED DREV-R-4161/79 NL

| OF |
ADA
080053

END
DATE
FILMED
2-80
DDC

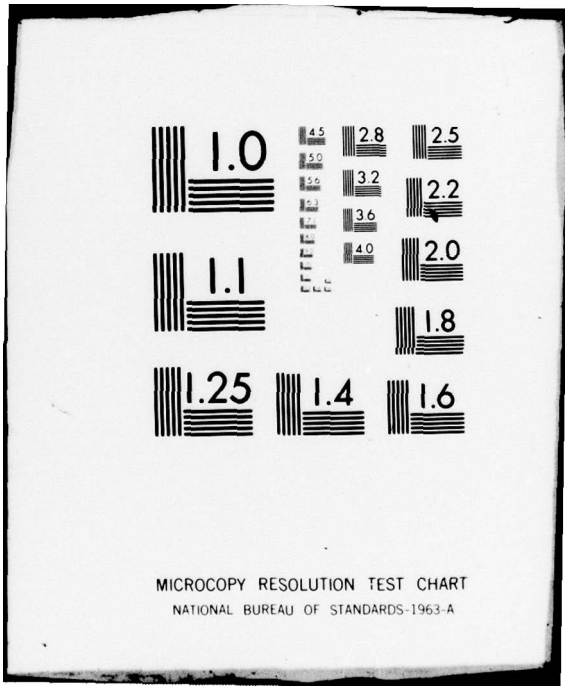
1.0
1.1
1.25
1.4
1.6
1.8
2.0
2.2
2.5
2.8
3.2
3.6
4.0
4.5
5.0
5.6
MICROCOPY RESOLUTION TEST CHART
NATIONAL BUREAU OF STANDARDS-1963-A

UNCLASSIFIED
UNLIMITED DISTRIBUTION

UNLIMITED DISTRIBUTION
ILLIMITÉE

CRDV RAPPORT 4161/79
DOSSIER: 3633H-004
OCTOBRE 1979

DREV REPORT 4161/79
FILE: 3633H-004
OCTOBER 1979

3
A-S.

AD A080053

LEVEL II

EXPERIMENTAL STUDY OF AN OPTICAL GUIDED-BEAM SPLITTER

D. Vincent

J.W.Y. Lit

P. Lavigne

G. Otis

DDC
RECEIVED
JAN 30 1980
A

DDC FILE COPY

Centre de Recherches pour la Défense
Defence Research Establishment
Valcartier, Quebec

BUREAU - RECHERCHE ET DÉVELOPPEMENT
MINISTÈRE DE LA DÉFENSE NATIONALE
CANADA

RESEARCH AND DEVELOPMENT BRANCH
DEPARTMENT OF NATIONAL DEFENCE
CANADA

NON CLASSIFIÉ
DIFFUSION ILLIMITÉE

80 1 21 141

CRDV R-4161/7
DOSSIER: 3633h-004

UNCLASSIFIED

(14) DREV-R-4161/79
FILE: 3633H-004

(6) EXPERIMENTAL STUDY OF AN OPTICAL GUIDED-BEAM SPLITTER,

(12) 39

by

(16) D./Vincent, J.W.Y./Lit, P./Lavigne and G./Otis

* Wilfrid Laurier University, Waterloo, Ontario

(11) Oct 79

CENTRE DE RECHERCHES POUR LA DEFENSE

DEFENCE RESEARCH ESTABLISHMENT

VALCARTIER

Tel: (418) 844-4271

Québec, Canada

October/octobre 1979

NON CLASSIFIE

404 945

JOB

RESUME

Nous avons mesuré la réflectivité R d'une séparatrice pour faisceau optique guidé. La méthode de fabrication, utilisant un fil mince comme masque, donne au guide plan une variation d'épaisseur de forme parabolique. Les résultats expérimentaux indiquent clairement que l'expression théorique $R=\tanh^2\delta$ décrit bien ce phénomène, surtout dans le cas d'un mode TM_0. Nous discutons également de quelques applications possibles de cette structure telles qu'un analyseur de polarisation et un sélecteur de modes. (NC)

ABSTRACT

Measurements on the reflectance R of a guided-beam splitter have been performed. The fabrication method, based on the use of a thin wire as a mask, produces a groove with a parabolic thickness profile in a planar waveguide. The experimental results demonstrate that the theoretical expression $R=\tanh^2\delta$ describes well the observed phenomena, especially when the TM_0 mode is incident on the groove. Additional applications of this device for polarization analysis and mode selection are also discussed. (U)

TABLE OF CONTENTS

RESUME/ABSTRACT i

1.0 INTRODUCTION 1

2.0 BEAM SPLITTER GEOMETRY AND FABRICATION 2

3.0 PHOTOGRAPHIC RESULTS AND OBSERVATIONS 7

4.0 MEASUREMENTS 12

4.1 Measurement of R and T 12
4.2 Expressions for δ with Different Profiles b(Z) 13
4.3 Parameter Fitting 15
4.4 Results 16

5.0 COMPARISON BETWEEN EXPERIMENTAL POINTS AND ADJUSTED THEORETICAL CURVES 21

6.0 DISCUSSION ABOUT THE PARAMETERS OBTAINED 24

6.1 Graphical Representation as a Function of b_2 24
6.2 Emergence of the Parabolic Profile 26
6.3 Disagreement of the TE_o Mode Results 28
6.4 Angular Response of the Beam Splitter for the TE_o and TM_o Modes 29

7.0 APPLICATIONS 30

7.1 Reflector and Beam Splitter 30
7.2 Angular Magnification 30
7.3 Mode Selector; Polarization Analyser 31

8.0 CONCLUSIONS 32

9.0 REFERENCES 33

FIGURES 1 to 14

1.0 INTRODUCTION

Some military applications of lasers require miniaturization of sources and of the associated optical circuitry. Such a miniaturization is possible using waveguide techniques; materials in thin film or slab form, suitable for propagation of a 10.6-μm guided beam, have been investigated since 1973. The interest was (and still remains) in constructing optical circuits directly compatible with mid-infrared radars.

One of the main components of these infrared radars is the local oscillator at 10.6 μm which has to be highly stable. A possible way of achieving the required stability is to build a very small waveguide laser with distributed feedback. This technique would lend itself to integration and would possibly give the high stability desired.

This work presents experimental results of a study on a beam splitter operating at optical frequencies and simulating a possible output coupler and splitter for such a waveguide laser. Some preliminary results and calculations have been presented elsewhere (Ref. 1). The technique is based on the fabrication, in a thin film (the waveguide), of a smooth-profile groove that acts as a "frustrated total reflection" filter via evanescent coupling of the guided mode.

The following sections present photographic results and measurements of reflectance and transmittance as functions of the incidence angle of the mode and the parameters of the splitter.

This work was initiated at the Département de physique, Université Laval, on January 1977 under contract No 8SR5-0072, "Conception et construction d'un prototype de laser à couche mince" and continued at DREV from July to December 1978 under PCN 33H04 "Miniaturization of Lasers".

2.0 BEAM SPLITTER GEOMETRY AND FABRICATION

As already shown in Ref. 1, the one-to-one correspondence that exists between the thickness b of a planar waveguide and the effective refractive index N of a propagating mode permits a bidimensional treatment of the wave propagation. In particular, continuous refraction in the plane of the waveguide along a suitably profiled groove may be applied to the design of a guided-beam splitter.

Using the mask shown in Fig. 1, we have succeeded in making planar waveguides with a gently sloped symmetric groove, (Fig. 2), on a glass substrate (Corning 7059). Figure 3 gives the calculated thickness profile obtained from the positions of the taper interference fringes taken in reflected (sodium) light with a Zeiss microscope. The important parameters that govern the groove shape are the wire radius R, the mask-substrate gap height h and the free-aperture thickness b_ℓ. The film surface slope at every point is denoted by tan α. The films, made by sputtering tantalum in a reactive atmosphere of oxygen and nitrogen, have a refractive index n adjustable via the relative gas concentration as described in detail in Refs. 2 and 3. The refractive index and thickness of the film are measured by the prism-coupler technique (Ref. 4).

An incident guided beam, in the YZ plane, may be divided into a reflected beam and a transmitted beam (Fig. 2a) if

$$N(b(Z_o)) = N(b(Z_o')) = N(b_1) \sin\theta \gtrsim N(b_2), \qquad [1]$$

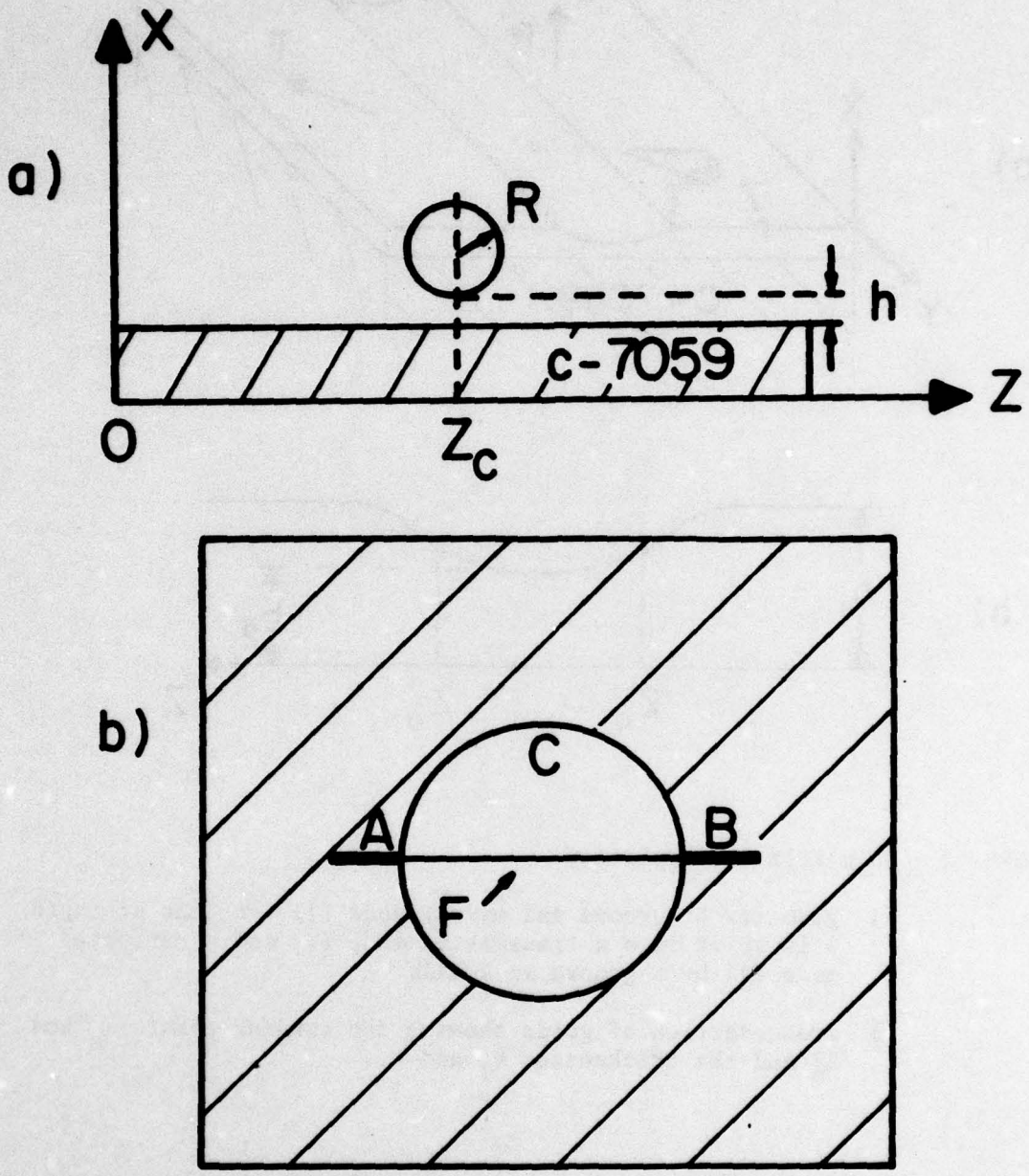

FIGURE 1 - Cylindrical mask
a) cylinder with radius R at a distance h from substrate
b) mask with chromel wire F and aperture C.

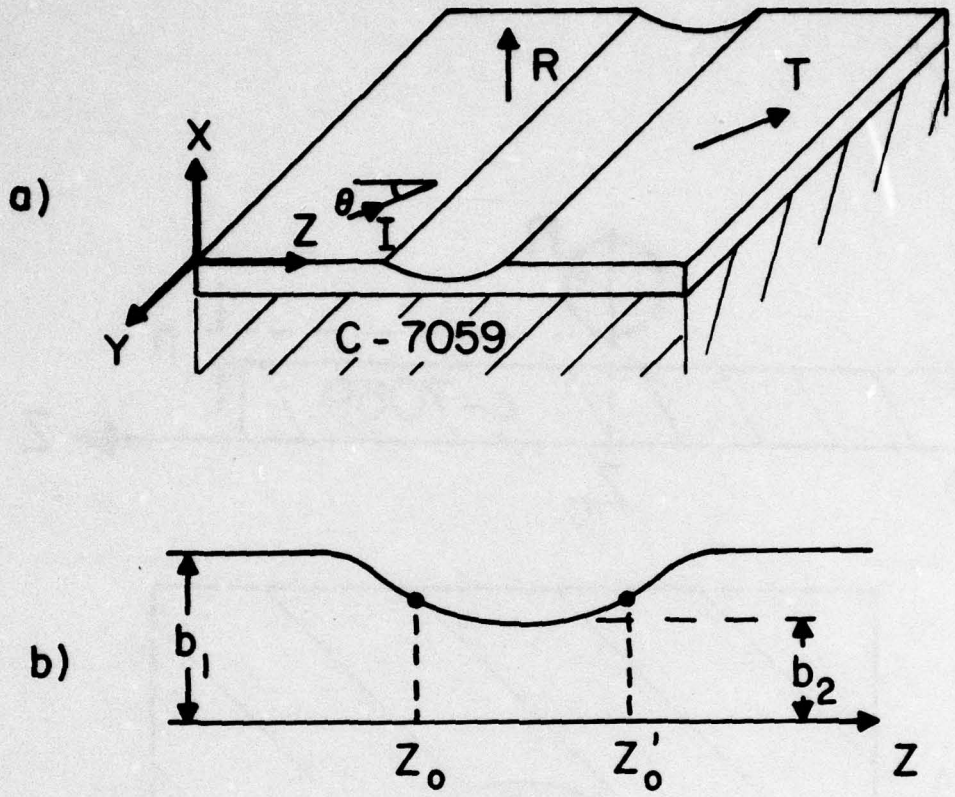

FIGURE 2 - Thin-film beam splitter

a) geometry of groove and waves: mode (I) incident at angle θ is split into a transmitted mode (T) and a reflected mode (R) by a groove in a film

b) cross-section of guide showing the turning points Z_o and Z_o' and the thicknesses b_1 and b_2.

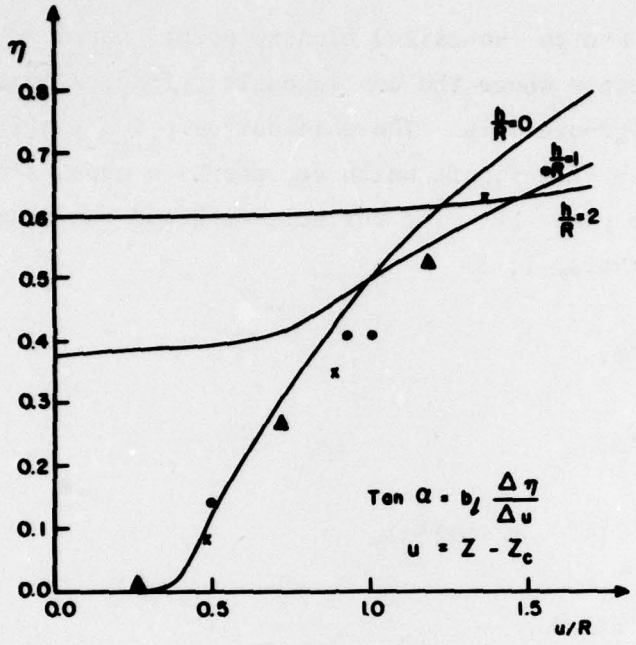

FIGURE 3 - Curves of thickness profiles produced by a cylindrical mask for different values of h/R. The experimental points correspond to three different films deposited with the same mask and h/R = 0.

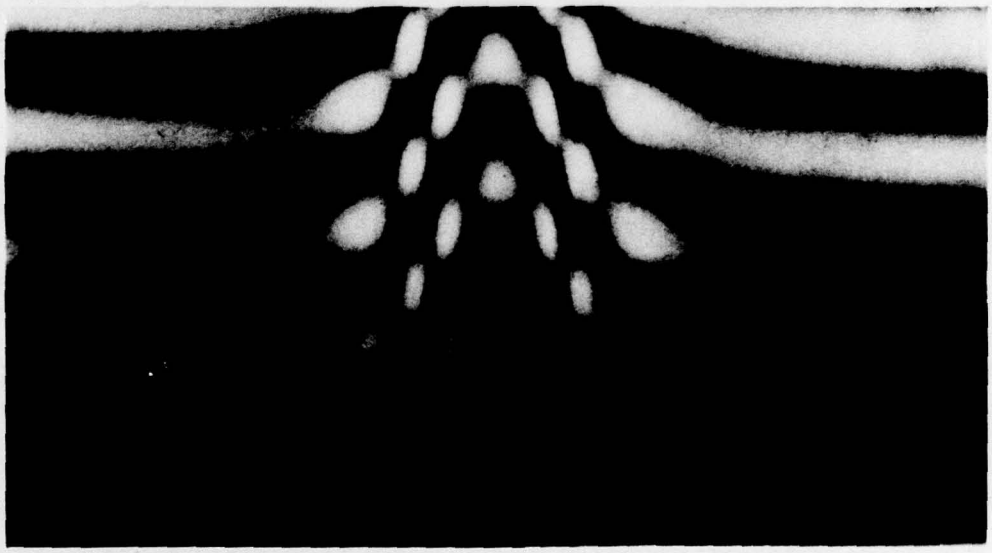

FIGURE 4 - Interference fringes showing the thickness profile fringes due to the groove and perpendicular fringes due to a Michelson interferometric objective.

where Z_o and Z_o' are the so-called turning points noted in Fig. 2. These are the points where the continuously refracted beam propagates parallel to the groove axis. The thicknesses b_1, b_2, $b(Z_o)$ and $b(Z_o')$ are also shown in this figure which represents a cross-section of the guide in the plane XZ. The reflectance R and the transmittance T are given by (Refs. 1, 3)

$$R = \tanh^2\delta, \qquad [2]$$

$$T = \operatorname{sech}^2\delta,$$

$$\text{with } \delta = k\int_{Z_o}^{Z_o'} (S^2 - N^2(b))^{\frac{1}{2}}dZ, \qquad [3]$$

where $S \equiv N(b_1) \sin\theta$

The argument δ is itself a function of θ, b_1, b_2 and of the groove profile between Z_o and Z_o'. Since coupling between the two turning points occurs via an evanescent wave, the distance $Z_o\ Z_o'$ has to be comparable to λ. Thus, the interesting region of the thickness profile in Fig. 3 is given by $R^{-1}u \lesssim R^{-1}\lambda \simeq 0.01$ (if R = 50 μm and $\lambda \simeq 0.6$ μm). The profile in this region cannot be determined from the taper fringe measurements since $\Delta b \simeq 4$ nm if the reflectance R = 1/2, and since the fringe separation is 147 nm (λ_{Na} = 589 nm and n = 2.0). Because $\Delta b/\lambda_{Na} \simeq 1/150$, even a Michelson interferometer in a microscope objective (Watson 10 X) cannot resolve this profile as shown in Fig. 4: the bright central region is about 25 μm wide and measurement of the thickness profile in a 1-μm width at the center of this region is impossible. Therefore, the profile b(u) must be estimated in this region and the calculated δ compared with measurements for each estimation; this will be the subject of Section 4.2.

3.0 PHOTOGRAPHIC RESULTS AND OBSERVATIONS

This section describes the various operation modes of this beam splitter with a He-Ne laser beam (Spectra Physics model 120, $\lambda \approx 0.6328$ μm) propagating in the waveguide. It has been found in Ref. 1 that ray trajectories in such an index profile are approximately parabolic. It is easy to show that if $S \approx N_2 \equiv N(b_2)$, the curvature increases if N_2 decreases. Figures 5a and 5b show the influence of b_2. In Fig. 5a, a TE_o mode incident on the splitter (b_1 = 480 nm, b_2 = 360 nm, n = 2.10) is turned more slowly than in Fig. 5b (b_1 = 612 nm, b_2 = 140 nm, n = 2.10). The transmitted and the reflected beams in Fig. 5b seem brighter at a certain distance from the splitter. This change in scattered intensity stems from the fact that the splitter has been made with two films as shown in Fig. 6: one film with the mask of Fig. 1b, covered with an extra film without the mask. The incident beam is coupled at A and split at B. When the reflected beam arrives at D, and the transmitted beam at C, the thickness reduction gives rise to an increase in the number of reflections at the film-air interface; this implies greater scattering. The effect is more pronounced when $N_1 - N_2$ is large or, in other terms, it is proportional to $\partial N/\partial b$. In particular, if $n_M \equiv n_{TM} > n_E \equiv n_{TE}$, the change in scattered intensity will be more apparent for TM modes. The use of this two-film technique to fabricate the device allows the control of b_1 and b_2 separately, but requires a change of mask which implied in our case that the first film was exposed to air before deposition of the second one. Therefore, a thin contamination layer may be formed in the process, but the guides obtained did not show excessive losses with respect to one-film guides.

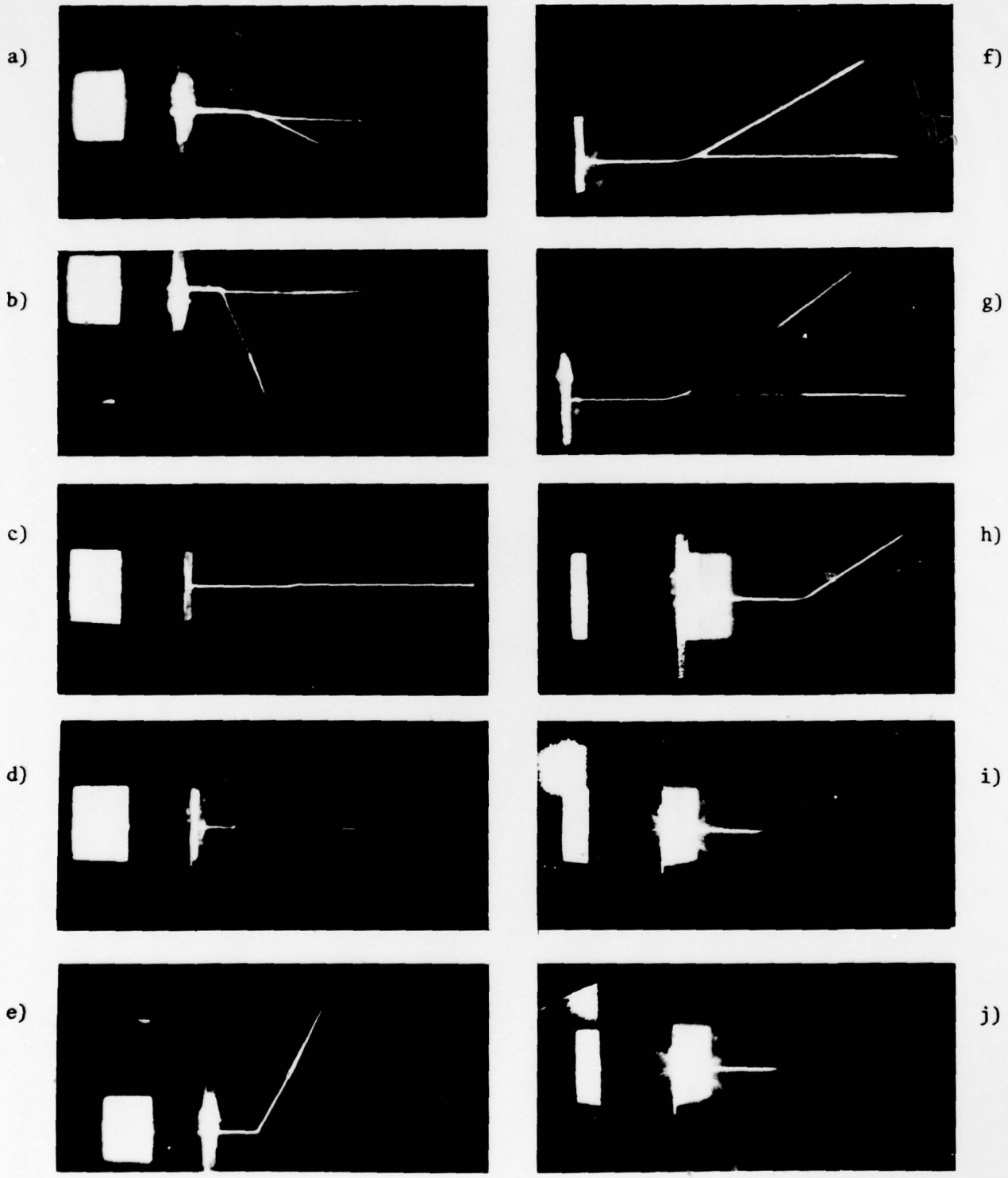

FIGURE 5 - Optical guided-beam splitters

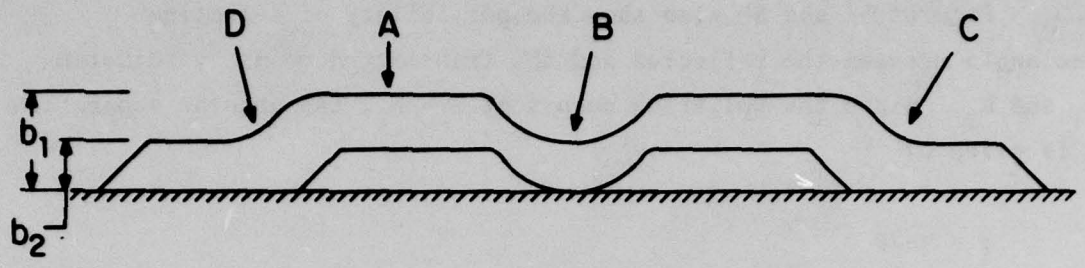

FIGURE 6 - Schematic diagram of two-film structure for the beam-splitter

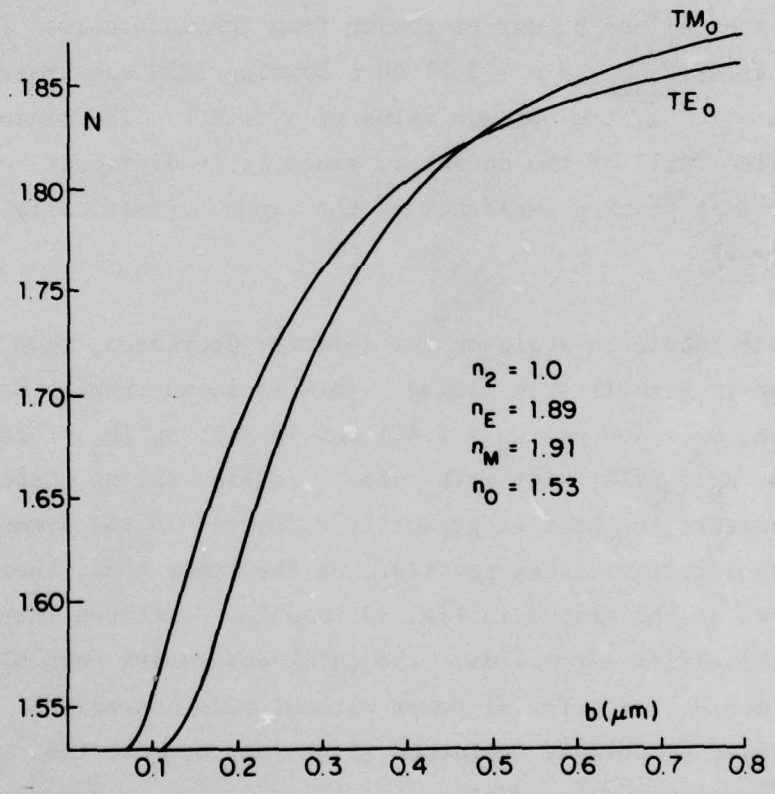

FIGURE 7 - TE_0 and TM_0 mode curves for a positive birefringent film

Figures 5a and 5b also show the possibility of selecting the angle between the reflected and the transmitted beams by adjusting b_1 and b_2. Since the splitting occurs at $S \simeq N_2$, the angular separation ψ is given by

$$\psi \simeq \pi - 2\theta$$

$$\simeq 2 \cos^{-1}\left(\frac{N_2}{N_1}\right). \qquad [4]$$

The thicknesses b_1 and b_2 may be chosen from the mode curves (Ref. 3). In a Ta_2O_5 film ($N_{1\ max} = n \simeq 2.1$) on a Corning 7059 substrate ($N_{2\ min} = n \simeq 1.53$), the maximum value of ψ is 86^o. The minimum value depends on the skill of the operator, since it is difficult to couple into the film at grazing incidence on the taper. Practically, in our case, $\psi_{min} \simeq 5^o$.

If the incidence angle on the splitter decreases, then $\delta \to 0$ and the beam is totally transmitted. This is shown in Fig. 5c (b_1 = 706 nm, b_2 = 406 nm, n_E = 1.89) and in Fig. 5d (b_1 = 612 nm, b_2 = 140 nm, n_E = 2.10) with a TE_o mode. In Fig. 5c, no insertion loss is apparent; the beam is gradually refracted in the symmetrical slow-varying effective index profile. On the other hand, there is a bright spot at the groove in Fig. 5d, and the scattered intensity is very much smaller afterwards. The thickness varies probably too rapidly to achieve transfer of power without mode conversion. This loss is smaller at oblique incidence (Fig. 5b), because the transition becomes more gradual.

If the incidence angle θ increases so that $\delta >> 1$, then $T \to 0$ and $R \to 1$, as seen in eq. 2. This is illustrated in Fig. 5e (b_1 = 612 nm, b_2 = 140 nm, n_E = 2.10) where a TE_o mode is totally reflected by continuous refraction along the groove. There is no visible loss at the splitter and this always occurs at total reflection for any value of b_2.

Figures 5f and 5g compare the splitting (approximately 3 dB) of TE_o and TM_o modes respectively, in a TaO_xN_y film (b_1 = 445 nm, b_2 = 267 nm, n_E = 1.88, n_M = 1.90). Since $n_M > n_E$, the variations in scattered intensity in going from one guide thickness to the other are greater for the TM_o case. The beams, slowly deviated by the nonuniform region, emanate on each side at equal angles ($\theta_i = \theta_r = \theta_t = 75^o$ for TE_o and $\theta_i = \theta_r = \theta_t = 71.5^o$ for TM_o) as this is a symmetrical effective index profile. The angular separation ψ is larger in the TM_o case because $n_M > n_E$. In fact, this film has a positive birefringence which is large enough to make the TE_o and TM_o mode curves cross each other (Fig. 7 for a typical example): consequently, $\partial N/\partial b$ is larger in the TM_o case. Then, for constant b_1 and b_2, $N_2/N_1 = 1 - \Delta N/N_1$ is smaller for the TM_o mode, leading to a larger ψ (eq. 4). The loss at the splitter (visible as a diffuse spot at the end of the substrate) is very small in both cases.

Finally, figs. 5h, i and j show the behavior of a TM_1 mode (in the same film as on photo f and g) when incident on the splitter. As the incidence angle decreases, the mode is totally reflected on photo h, partially reflected and partially converted to substrate modes on photo i, and cut off on photo j. These three photos show what happens if b_2 is too small: the mode is cut off before splitting occurs. Nevertheless, with $b_2 > 350$ nm, splitting of the TM_1 mode is possible. This applies to every mode if b_2 is larger than the cut off thickness for that mode; then, the behavior is as shown in photos a to e.

4.0 MEASUREMENTS

4.1 Measurements of R and T

To check the validity of eqs. 2 and 3, the reflectance and transmittance of the splitter have been measured with respect to θ and b_2 (with b_1 almost constant). Only the fundamental TE_o and TM_o modes were considered. A fiber bundle collected the light scattered from the waveguide in each beam. Synchronous detection at 1.034 kHz was used with a lock-in amplifier (Princeton Applied Research model HR-8). The wavelength was $\lambda = 0.6328$ μm.

At the beginning, it was clear that the measurement of the incident beam power would be very difficult at several θ. This was due primarily to the scattering at the prism edge, to the bulkiness of the fiber bundle and prism coupler, and to the possibly small distance between the prism and the groove. The insertion loss has been measured and found smaller than the detection system accuracy (typically 3%), so that only the measurement of the transmitted and the reflected beams intensities was required.

The detector is placed alternately on the reflected beam (I_R) and on the transmitted beam (I_T) at the same distance from the splitting point in both cases. Since it is always the same mode in the same film, propagation loss does not have to be taken into account. The angle $\theta_{\frac{1}{2}}$ for which $R = T = 1/2$ (found by trial and error) is noted and, thereafter, I_R and I_T are measured as functions of $\theta - \theta_{\frac{1}{2}}$. Finally, the experimental value $\delta_{exp} = \tanh^{-1}\sqrt{R}$ is determined and used to check if this experimental curve may be deduced from a given N(Z) profile. If so, it is concluded that eqs. 2 are representative of the device under consideration.

4.2 Expressions for δ with Different Profiles b(Z)

To evaluate δ as given by eq. 3, we must specify the functions N(b) and b(Z). In the following, we take

$$N^2 = N_2^2 + \frac{\partial N^2}{\partial b}\Big|_{b_2} (b-b_2)$$

$$= N_2^2 + m_2 (b-b_2) \qquad [5]$$

as an approximation to the mode curve near the splitting point ($S \simeq N_2$ and $b \simeq b_2$).

a) Constant Profile (Fig. 8a)

Let us assume that $b(Z) = b_2$ if $|Z| < c/2$, and $b(Z) = f(Z)$, if $|Z-Z_o| < \ell$ and $|Z-Z_o'| < \ell$, with $\ell \ll c$ and $|f(Z)-b_2| \to 0$. Then, the integration in eq. 3 runs practically from - c/2 to c/2 (the interval ℓ is used only to generate a turning point) and gives, using $N^2 = N_2^2$,

$$\delta = kc\ (S^2 - N_2^2)^{\frac{1}{2}}. \qquad [6]$$

b) Linear Profile (Fig. 8b)

Putting $b(Z) = b_2 + (\tan \alpha)\ Z$, if $|Z| \geq \ell$, and $b(Z) = f(Z)$, if $|Z| < \ell$, still with the assumptions that $2\ \ell \ll |Z_o - Z_o'|$ and that $|f(Z)-b_2| \to 0$ if $|Z| < \ell$, then

$$N^2 = N_2^2 + (m_2 \tan \alpha)\ |Z|$$

and

$$\delta = (4\ k/3m_2 \tan \alpha)\ (S^2 - N_2^2)^{3/2}. \qquad [7]$$

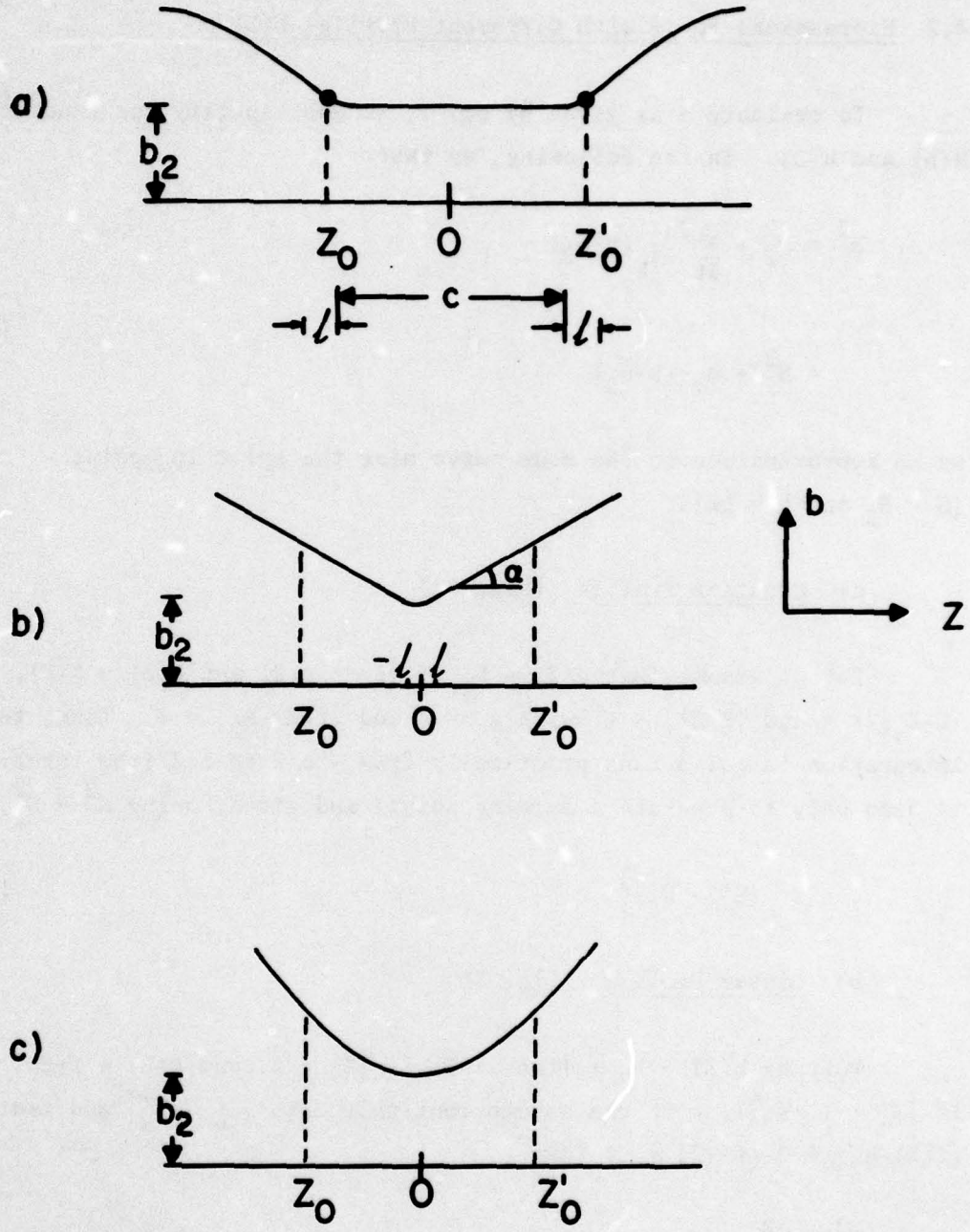

FIGURE 8 - Defining the profiles used to calculate δ:
a) constant b) linear c) parabolic

c) Parabolic Profile (Fig. 8c)

Finally, let $b(Z) = b_2 + g_p Z^2$ if $2|Z| < |Z_o - Z'_o|$, then

$$N^2 = N_2^2 + m_2 g_p Z^2$$

and

$$\delta = (\pi k / 2\sqrt{m_2 g_p})\ (S^2 - N_2^2). \qquad [8]$$

4.3 Parameter Fitting

To determine c, tan α and g_p in eqs. 6, 7 and 8, a plot of $R(\theta, N_1, N_2)$ is used with a linear development around $\theta = \theta_{\frac{1}{2}}$: the slope of these curves around $\theta = \theta_{\frac{1}{2}}$ leads directly to a value of the parameters. With these empirical values of c, tan α and g_p, it is possible to calculate $R(\theta, N_1, N_2)$ and to compare it with the experimental curves.

Using $\theta = \theta_{\frac{1}{2}} + \varepsilon$ with $\varepsilon << 1$ and developing S to the first order, one obtains

$$S^2 - N_2^2 \simeq N_1^2 \sin^2\theta_{\frac{1}{2}}\ (1 + \varepsilon \cot \theta_{\frac{1}{2}})^2 - N_2^2. \qquad [9]$$

Experimentally, $\pi/2 > \theta_{\frac{1}{2}} \geq \pi/4$, since $\theta_{min} = 1/2\ (\pi - \psi_{max})$, and $\psi_{max} < \pi/2$, so that $0 < \cot \theta_{\frac{1}{2}} \leq 1$ and [9] becomes

$$S^2 - N_2^2 \simeq S_{\frac{1}{2}}^2 - N_2^2 + 2 S_{\frac{1}{2}}^2 \varepsilon \cot \theta_{\frac{1}{2}}. \qquad [10]$$

Substituting this result into eqs. 6-8 leads to

$$\underline{\text{constant profile}}: \quad (\delta/\delta_{\frac{1}{2}})^2 = 1 + 2\, S_{\frac{1}{2}}^2 \cot \theta_{\frac{1}{2}} \left(\frac{kc}{\delta_{\frac{1}{2}}}\right)^2 \varepsilon, \qquad [11]$$

$$\underline{\text{linear profile}}: \quad (\delta/\delta_{\frac{1}{2}})^{2/3} = 1 + 2\, S_{\frac{1}{2}}^2 \cot \theta_{\frac{1}{2}} \left(\frac{4k}{3\delta_{\frac{1}{2}}\, m_2 \tan \alpha}\right)^{2/3} \varepsilon, \qquad [12]$$

$$\underline{\text{parabolic profile}}: \quad (\delta/\delta_{\frac{1}{2}}) = 1 + \frac{\pi k\, S_{\frac{1}{2}}^2 \cot \theta_{\frac{1}{2}}}{\sqrt{(m_2\, g_p)}\, \delta_{\frac{1}{2}}} \varepsilon. \qquad [13]$$

The value of $\delta_{\frac{1}{2}} = 0.8814$ is given by $R = \tanh^2 (\delta_{\frac{1}{2}}) = 1/2$. Measurements of $R(\varepsilon)$ and $\theta_{\frac{1}{2}}$ for a given couple (b_1, b_2) yield values of $\delta_{exp} = \tanh^{-1} \sqrt{R}$. The curves $(\delta_{exp}/\delta_{\frac{1}{2}})^q$ with respect to ε (q equal to 2, 2/3 and 1, respectively) are straight lines around $\varepsilon = 0$ and their slopes give $\lambda^{-1}c$, $\tan \alpha$ and $2\, g_p$.

4.4 Results

Figure 9 shows a sample of the results obtained, in which the incident power on the splitter and the propagation loss ($\simeq$ 1 dB/cm) have been taken into account. It is obvious that $R + T \simeq 1$ as it should be. The curves are shown only as a visual aid without any use of the above fitting method.

Figures 10 and 11 illustrate the experimental results obtained to date in the form given by eqs. 11 to 13. Figure 10 represents the measurements on five different films for the TM_o mode, and, Fig. 11, on three films for the TE_o mode. The angle $\Delta\varepsilon$ has an arbitrary origin. It is easy to find the slope at $\delta/\delta_{\frac{1}{2}} = 1$ in each case. Moreover, the angular range is very similar from one film to the other, since the points are well grouped.

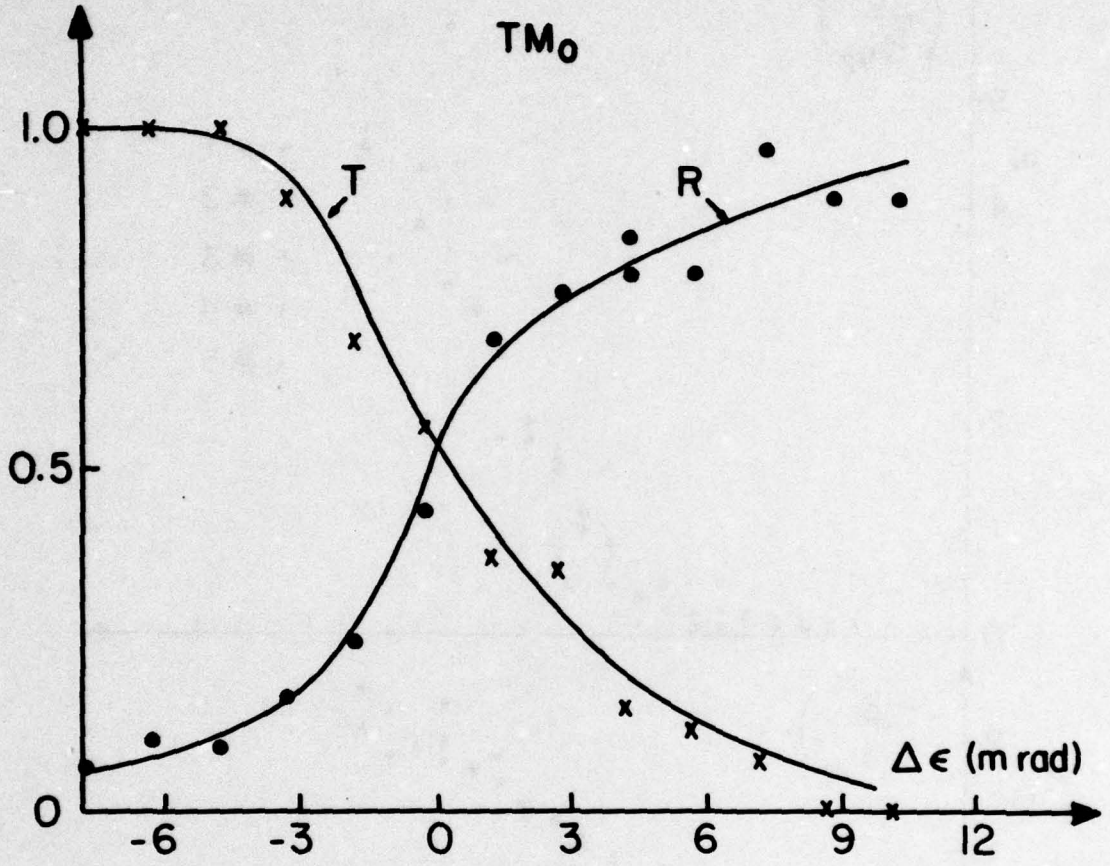

FIGURE 9 - Experimental results for the reflection coefficient R and transmission coefficient T as functions of angular deviation $\Delta\epsilon = \theta - \theta_1$ for a TM_0 mode. The curves show the mean behavior of the results.

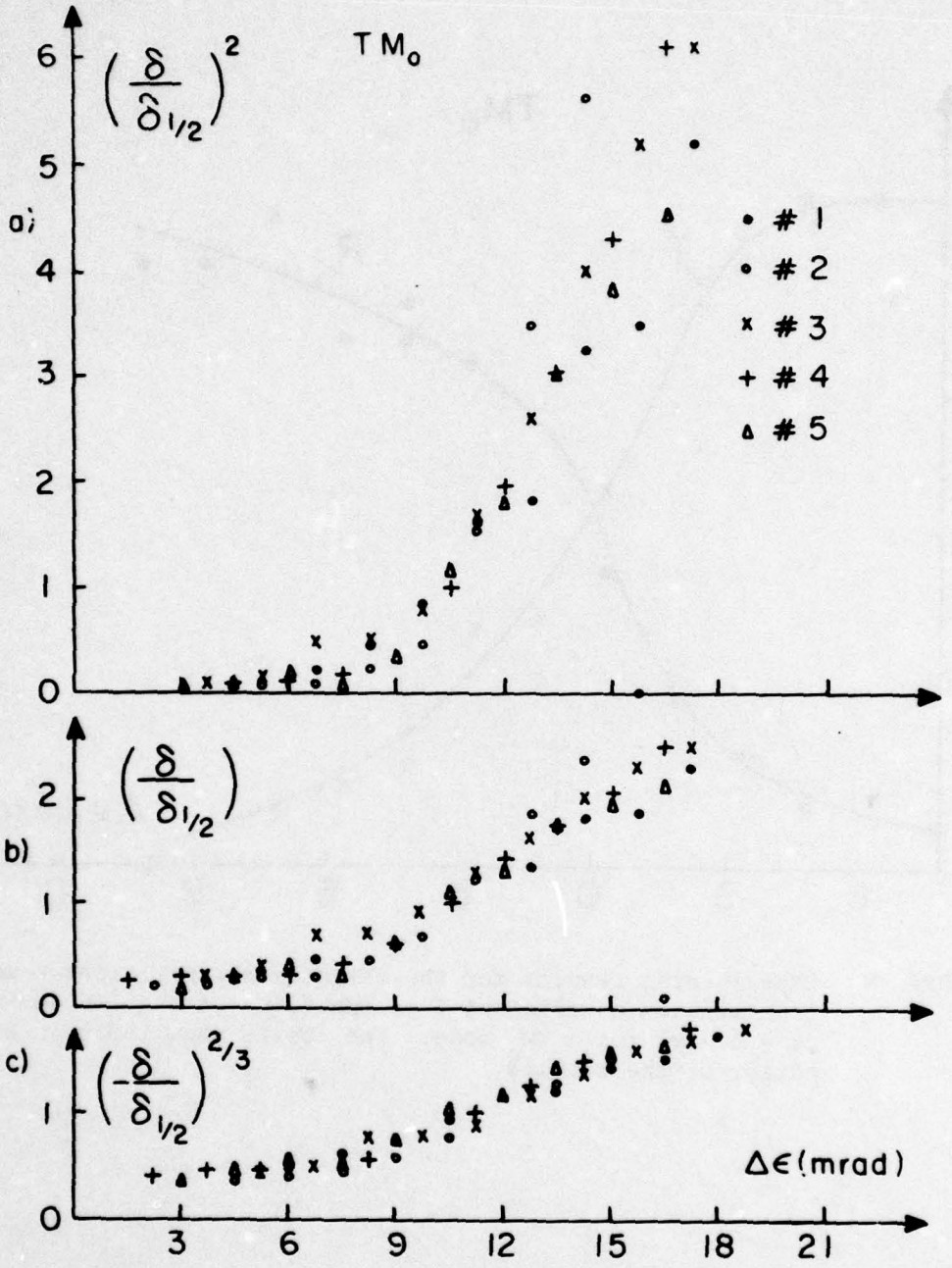

FIGURE 10 - Adjustment of the parameters for the TM_0 mode for a) constant profile b) parabolic profile c) linear profile

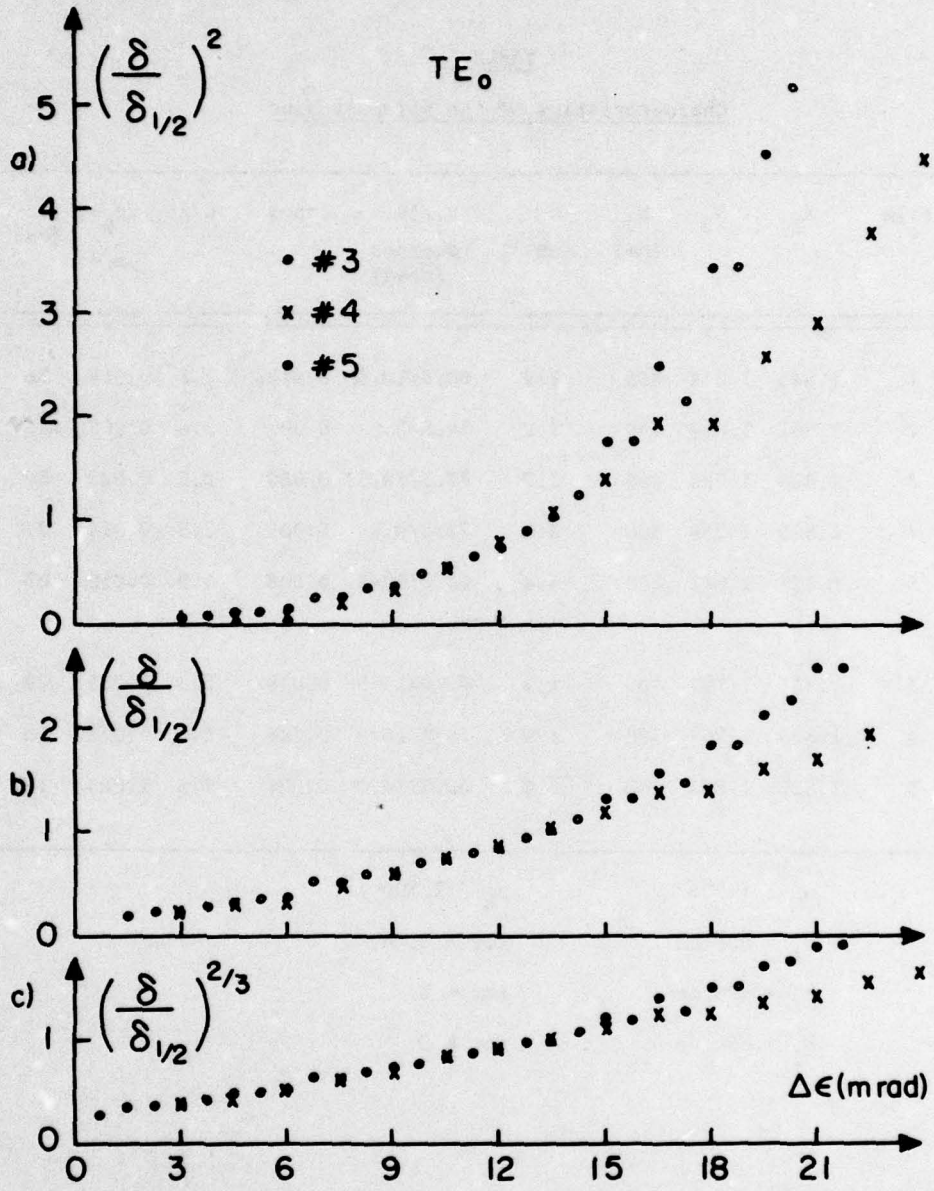

FIGURE 11 - Adjustment of the parameters for the TE_0 mode for a) constant profile b) parabolic profile c) linear profile

TABLE I

Characteristics of the films studied

Mode	Film #	N_1	N_2	b_2 (nm)	m_2 (μm^{-1})	$\theta_i/\Delta\theta$ (degrees)/(mrad)	tan α	c/λ	$2g_p$ (μm^{-1})	ρ (μm)
TM_o	1	1.843	1.818	455	1.2	80.5/10.5	0.012(5)	2.8	0.018	56
	2	1.861	1.824	440	1.2	78.5/7.5	0.007	3.6	0.008	125
	3	1.828	1.785	400	1.7	77.5/10.5	0.009	2.5	0.020	50
	4	1.825	1.736	300	3.0	72.0/9.0	0.007	2.3	0.013	77
	5	1.827	1.642	200	4.4	64.0/10.5	0.008	1.9	0.016	63
TE_o	3	1.831	1.797	400	1.3	79.0/13.5	0.018	2.3	0.035	29
	4	1.825	1.763	300	1.9	75.0/16.5	0.028	1.5	0.075	13
	5	1.829	1.702	200	3.2	68.5/14.0	0.024	1.3	1.083	12

$n_M \sim 1.906$ $\quad$ $n_E \sim 1.890$

$b_1 = 500$ nm $\quad$ for # 3, 4, 5

$b_1 = 590$ nm $\quad$ for # 1

$b_1 = 650$ nm $\quad$ for # 2

The characteristics of the various films with the corresponding parameter values are summarized in Table I. N_2 has been set equal to $S_{\frac{1}{2}}$; this value, compared to $N(b_2)$ taken from a mode curve generated from the value of n_{film} and evaluated at the value of b_2 listed in Table I, is accurate to the third decimal. This accuracy is comparable to that of the measurement of b_2 and shows that $S_{\frac{1}{2}} \simeq N_2$ effectively. The symbol ρ in Table I designates the radius of the osculating circle about $Z = 0$, for the parabolic profile. This radius is equal to the local radius of curvature of the parabola $b(Z)$ which is itself given by $(2g_p)^{-1}$ because $\partial b/\partial Z << 1$. The value of m_2 has been found directly from the mode curves $N^2(b)$, about $b = b_2$ for each n_{film} and each polarization. Finally, the angle range $\Delta\theta$ for which R goes from 10% to 90% is also noted. It is clear that the average range for TE_o (14.5 mrad) is greater than that for TM_o (9.5 mrad).

5.0 COMPARISON BETWEEN EXPERIMENTAL POINTS AND ADJUSTED THEORETICAL CURVES

Figures 12 and 13 show the experimental points, and the three adjusted curves at $R = 1/2$, for films #3 and #5, respectively. It is seen, from these figures, that the agreement is better for the TM_o mode and for the parabolic and the linear profiles which give similar curves. The constant profile does not fit the experimental points for $R \lesssim 0.3$; however, it seems more applicable for the TM_o mode with $R > 0.5$.

Although the experimental values of $R_{TE_o}(\varepsilon)$ are, in general, greater than those of the adjusted curves, the agreement is good within an interval ± 0.2 around $R = 1/2$. If $R > 1/2$, the slope $dR/d\varepsilon$ of the experimental results is larger than that of the adjusted curves.

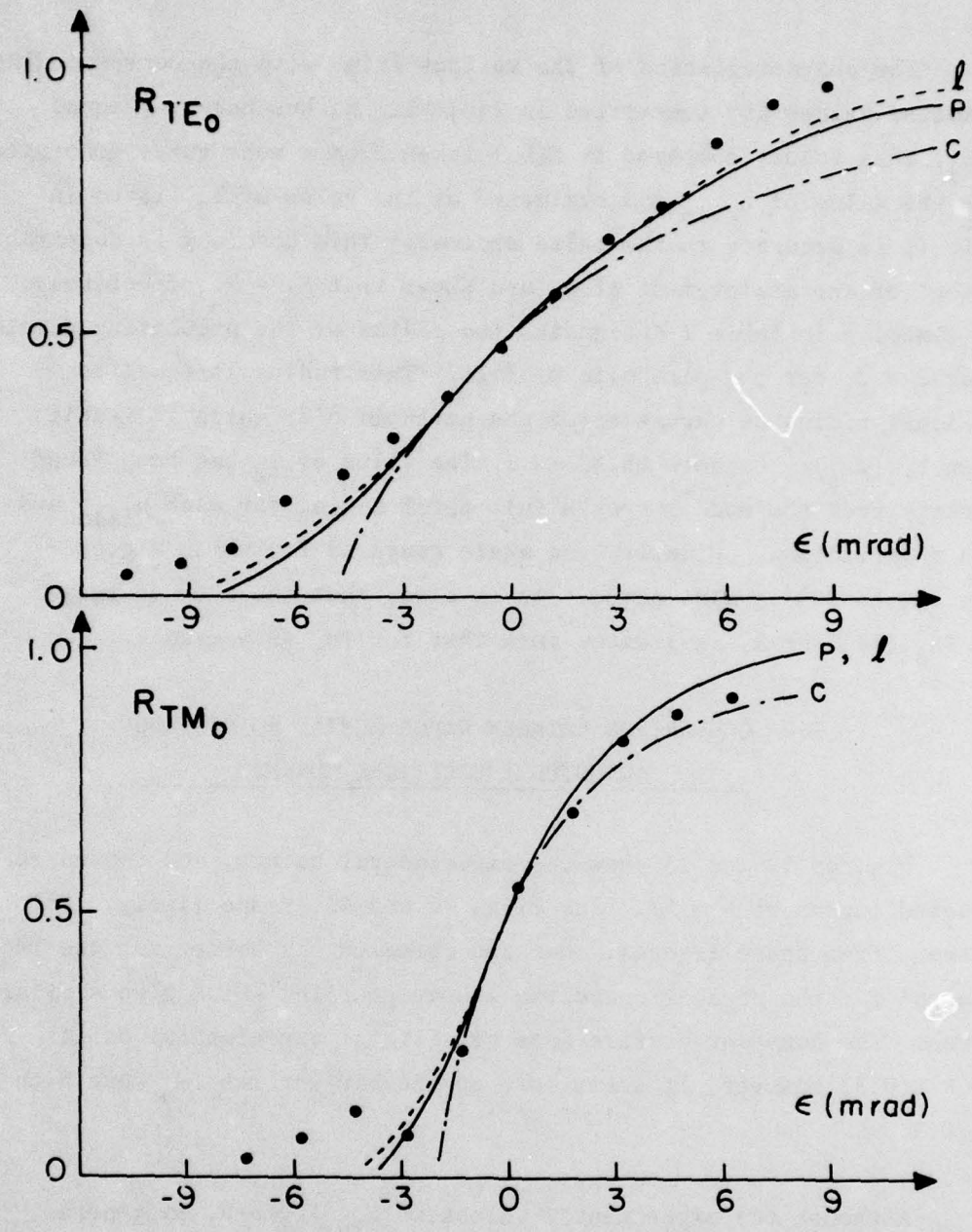

FIGURE 12 - Coefficient of reflection as a function of ε for TE_0 and TM_0 modes for film sample #3. Points are experimental results and curves are adjusted theoretical curves. The letters ℓ, p and c represent linear, parabolic and constant profiles.

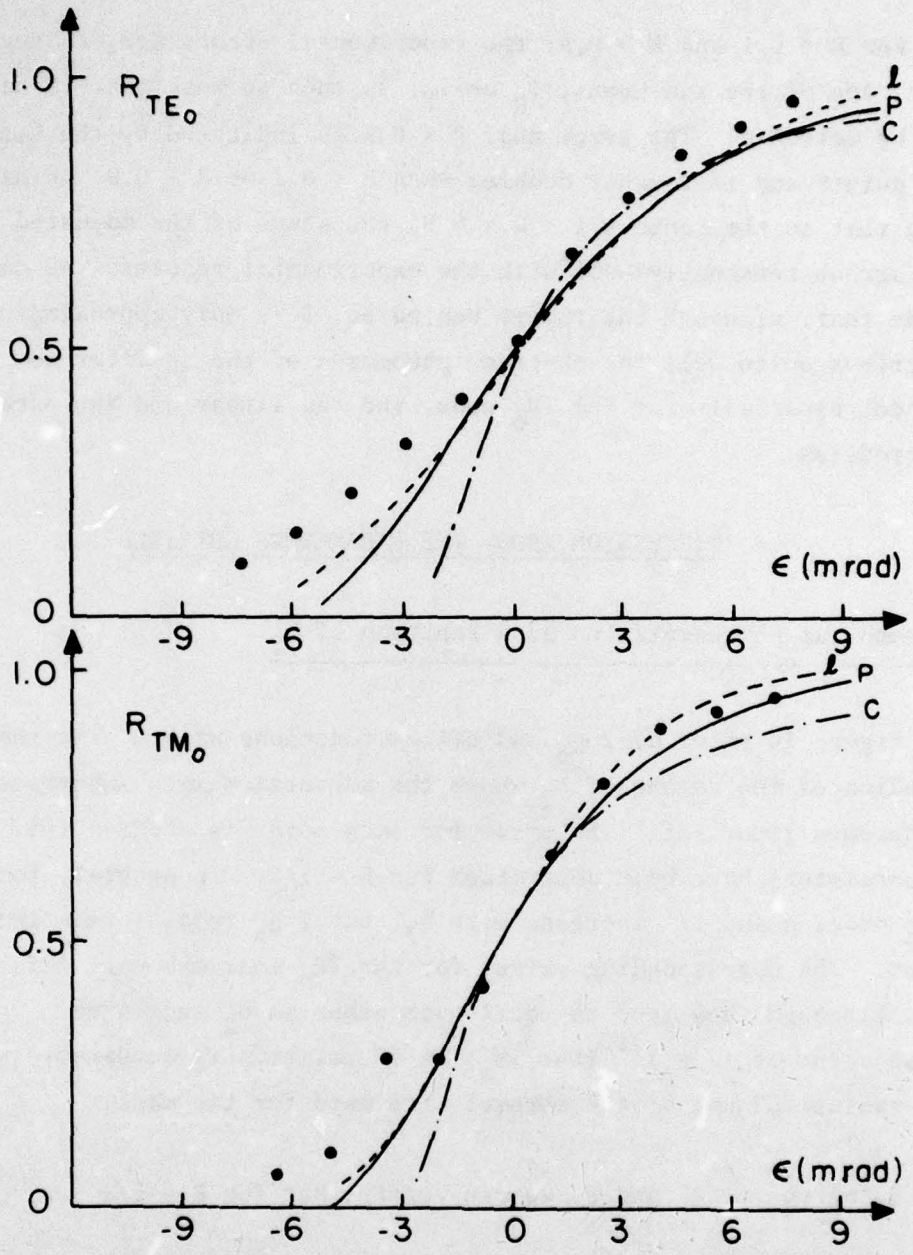

FIGURE 13 - Coefficient of reflection as a function of ε for TE_o and TM_o modes for film sample #5. Points are experimental results and curves are adjusted theoretical curves. The letters ℓ, p and c represent linear, parabolic and constant profiles.

For $R < 0.1$ and $R > 0.9$, the experimental errors are greater. In fact, one of the two beams, I_R or I_T, is then so weak that it can barely be detected. The error near $R = 0.5$ is indicated by the size of the points and is roughly doubled when $R < 0.1$ or $R > 0.9$. Finally, we note that in the range $0.1 < R < 0.9$, the shape of the adjusted curves agrees reasonably well with the experimental results. We can conclude that, although the theory behind eq. 2 is only approximate, it describes quite well the observed phenomena of the splitter we have made, especially for the TM_o mode, and the linear and the parabolic profiles.

6.0 DISCUSSION ABOUT THE PARAMETERS OBTAINED

6.1 Graphical Representation as a Function of b_2

Figure 14 shows α, $2\,g_p$ and c/λ as functions of b_2. The shaded zone indicates the values of b_2 where the conversion into substrate modes becomes important. The error for each point is about ± 10%. These parameters have been determined for $R = 1/2$. In general, for the TM_o mode, α and c/λ increase with b_2, but $2\,g_p$ remains relatively constant. The corresponding values for the TE_o mode are very different, although they tend to equal each other as b_2 increases. The mean value of $(2\,g_p)^{-1}$ (for TM_o) is 67 μm; this is comparable to the radius (52 μm) of the chromel wire used for the mask.

Using eqs. 6, 7 and 8, we can verify that for $R = 1/2$

$$\alpha^{-1} g_p\, c = (3/16)\pi^2 \simeq 1.85. \qquad [14]$$

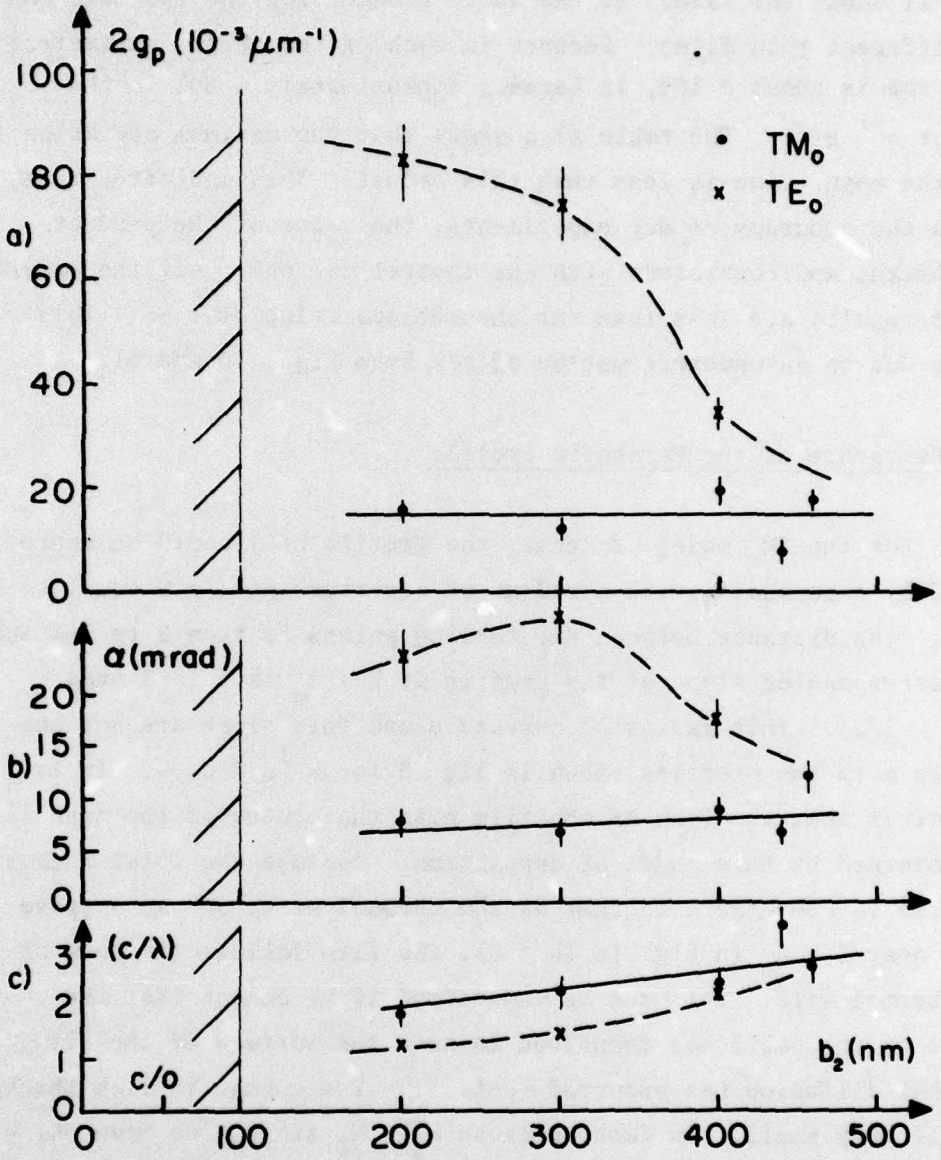

FIGURE 14 - Graphs of
a) $2g_p$ b) α c) c/λ
as functions of b_2. The shaded region (b_2 < 100 nm) shows values of b_2 for which conversion into substrate modes is not negligible. The cut-off thickness is indicated by c/o.

Table II shows the values of the above product for the two modes and for different thin films. Because in each of the three parameters the error is about ± 10%, it becomes approximately ± 30% in the product $\alpha^{-1}\, g_p\, c$. The table also shows that the maximum deviation from the mean value is less than this amount. This indicates that, within the accuracy of our experiments, the value of the product is constant and consistent with the theoretical one. All the experimental results are less than the theoretical value of 1.85. This may be due to an underestimation of c/λ from Figs. 10 and 11.

6.2 Emergence of the Parabolic Profile

For the TM_o mode, at least, the profile b(Z) could be represented by a parabola, with a radius of curvature at Z = 0 equal to 67 μm. The distance between the turning points is then 2 to 3 λ and the corresponding slope of the profile at $Z = Z_o$ is 7 to 8 mrad (at R = 1/2). This radius of curvature and this slope are not compatible with the profiles shown in Fig. 3 for $R^{-1}u \lesssim 0.04$. It is then clear that the form of the film near the center of the mask is not governed by this model of deposition. Because the local radius measured is comparable to that of the chromel wire, we can suppose that, near $Z = Z_o$ in Fig. 1a ($h \simeq 0$), the film follows the form of the chromel wire. This can be understood if we accept that the source of the particles deposited is near the surface of the film, and that diffusion has occurred (Ref. 5). The change in film thickness is very small. In fact, because $S_{\frac{1}{2}} = N_1 \sin \theta_{\frac{1}{2}}$, we have $\Delta S_{\frac{1}{2}} = S_{\frac{1}{2}} - N_2 \simeq N_1 \cos \theta_{\frac{1}{2}}\, \Delta\theta_{\frac{1}{2}}$ with $\Delta\theta_{\frac{1}{2}} = \frac{1}{2}\,\Delta\theta$ where Δθ is given in Table I. Typically, $\Delta S_{\frac{1}{2}} \simeq 4 \times 10^{-3}$. With a parabolic profile (Section 4.2c), $2N_2\, \Delta S_{\frac{1}{2}} \simeq m_2\, g_p\, Z_{\frac{1}{2}}^2$ which gives

$$Z_{\frac{1}{2}} = \frac{c}{2} = \left(\frac{2N_2\, \Delta S_{\frac{1}{2}}}{m_2\, g_p} \right)^{\frac{1}{2}} \qquad [15]$$

TABLE II

Verification of the consistency of the results obtained with the two modes in the different films

Mode	Film #	$\alpha^{-1} g_p c$
TM_o	1	1.3
	2	1.3
	3	1.8
	4	1.4
	5	1.2
TE_o	3	1.4
	4	1.3
	5	1.4
Average		1.4 ± 0.2

The value of the above expression is typically 0.8 μm, or again $c/\lambda \simeq 2.5$ (λ = 633 nm), which is approximately the mean value for the TM_o mode in Fig. 14c. Moreover, $2N_2 \Delta S_{\frac{1}{2}} = m_2 \Delta b_{\frac{1}{2}}$ which gives

$$\Delta b_{\frac{1}{2}} = 2N_2 \Delta S_{\frac{1}{2}}/m_2. \qquad [16]$$

This has a typical value of about 4 nm. We note that, for the sodium line, this value of $\Delta b_{\frac{1}{2}}$ is equivalent to $\lambda/150$, a high precision compared with that obtained with classical interferometry. We could also suppose that a migration phenomenon along the film surface is responsible for such a small Δb.

It can be concluded that the method of deposition used always gives a parabolic profile (quasi circular) for $R^{-1}u \leq 0.04$, if $h \simeq 0$. Finally, because the interval Δu is small, the linear approximation for the profile is also valid.

6.3 Disagreement of the TE_o Mode Results

It has been noted that, as b_2 increases, the values of α, c/λ and $2g_p$ of the TE_o mode approach those of the TM_o mode. Moreover, c/λ increases with b_2, which means that the distance $\overline{Z_o\ Z'_o}$ between the turning points, measured when $R \simeq 1/2$, increases also. It seems that this distance is too small in the case of a TE_o mode for the theoretical model to be true (Refs. 1, 3). In other words, $\overline{Z_o\ Z'_o}$ might be too small for the first order asymptotic development of the Airy functions between those two points to be true. That development would be valid for B_i (w), if (w) ≥ 0.5 and for A_i (w), if (w) ≥ 1 (Ref. 6). Now $N^2 = N^2\ (Z_o) + m_o\ \Delta b$ and, if we suppose that $\Delta b \simeq - \alpha\ \Delta Z$ then,

$$w \simeq (k^2\ \alpha\ m_o)^{1/3}\ \Delta Z. \qquad [17]$$

At the point Z_o, because $S_1 \simeq N_2$, $m_o \simeq m_2$ and we can use the values in Table I. Because $w \geq 1$, this leads to

$$\Delta Z = c/2 \geq (k^2\ \alpha\ m_2)^{-1/3}\ . \qquad [18]$$

If $m_2 = 2\ \mu m^{-1}$, $\alpha = 10$ mrad and $\lambda = 0.633\ \mu m$, eq. 18 gives $\Delta Z > 0.8\ \mu m$ or $c/\lambda \geq 2.5$.

For TM_o, c/λ varies between 2 and 3; as for TE_o, it can become as small as 1.2, it is, therefore, necessary to use the complete form of the Airy function. However, even though the results for the parameters for the latter mode are not in good agreement, Figs. 12 and 13 show that the $R(\varepsilon)$ curves reproduce fairly well the forms predicted by our theoretical model. This shows that $R(\varepsilon)$ is less sensitive to the approximation made than the $b(Z)$ profile.

6.4 Angular Response of the Beam Splitter for the TE_o and TM_o Modes

It has been said that the average interval $\Delta\theta$ necessary for R to vary from 0.1 to 0.9 is 14.5 mrad for TE_o and 9.5 mrad for TM_o. The He-Ne laser used throughout this work has a divergence of 1.7 mrad. Its beam was directed by a lens (focal length = 167 mm) onto the surface of a prism placed on the film and focussed at an angle of about 12 mrad. This beam divergence is projected onto the film (Ref. 6), resulting in a maximum beam divergence of 3 mrad inside the film. It is, therefore, evident that the $\Delta\theta$ at the beam splitter is not due to the beam divergence, but is caused by the coupling phenomenon. By allowing N_2 to vary with Y, i.e., a nonuniform groove in the Y direction, it is possible to make a beam splitter limited by the beam divergence. But this presents many more experimental difficulties.

7.0 APPLICATIONS

7.1 Reflector and Beam Splitter

The most evident application is the fabrication of a reflector ($\delta > 2$) or a 3 dB beam splitter ($\delta \simeq 0.88$) for an incident mode; a small angular adjustment will produce the desired result.

The working of this beam splitter differs significantly from that proposed by Tsang and Wang (Ref. 8). Their device was made of a crystalline substrate (silicon) in which a groove was produced by preferential etching, using an ionic beam. The analysis we have used here is not applicable to this case. The present theory is valid only when the parameters change slowly whereas their splitter had (Ref. 8) $|\nabla b| = \tan \alpha \simeq 1.4$. Moreover it did not function by coupling evanescent waves but by a process which is similar to the reflection on a dielectric mirror. A very large angular response was so obtained: the ratio R/T changes from 0.5 to 1.5 over an interval $\Delta\theta \simeq 12^{o}$.

7.2 Angular Magnification

Because eq. 4 allows ψ to be chosen and because the interval $\Delta\theta$ is quite small for $0.1 < R < 0.9$, we can have angular displacement magnification by choosing a large ratio $\psi/\Delta\theta$. In our case, this ratio varies from 8 to 150. For a thin-film acousto-optical deflector, if $2\theta_B = \lambda_g/\Lambda \simeq 60$ mrad between order 0 and order + 1, such a beam splitter can transmit one order and reflect the other, resulting in separating the two beams wide apart spatially. The symbols used above are θ_B = Bragg angle, Λ = acoustic wavelength, and Λ_g = guided wavelength. The Λ used corresponds to a frequency around 500 MHz.

7.3 Mode Selector, Polarization Analyzer

It has been noted above that $\theta_{\frac{1}{2}} \simeq \sin^{-1} (N_2/N_1)$. In general, for a given (b_1, b_2) pair, the values of N_1 and N_2 change from one mode to the other. It follows that $\theta_{\frac{1}{2}}$ will also be different for each mode guided by the film. Also, for a given mode, the beam incident with $\theta \leq \theta_{\frac{1}{2}}$ will be split into two parts: the chosen mode and lower order modes will be transmitted, while the higher order modes will be reflected (or coupled to substrate if $S \leq N_2 = n_s$ for those modes). Thus, the present beam splitter will act as a high-pass filter (in transmission) if we consider $1/\lambda_g$, where λ_g is equal to λ/N_1.

By using two suitable beam splitters, we can make a band-pass filter. The discrimination rate in N of such a filter can be estimated in the following manner. If θ is the angle of incidence, $\Delta S = \sin\theta \, \Delta N_1$. Also $\Delta S = N_1 \cos\theta \, \Delta\theta$, where $\Delta\theta$ is the angular response of the beam splitter. Thus

$$\Delta N_1 \simeq N_1 \cot\theta \, \Delta\theta = N_1 (N_1^2 - N_2^2)^{\frac{1}{2}} \Delta\theta/N_2.$$

If $\Delta\theta$ does not vary very much with N_1 and N_2 (this seems to be true by examining Table I) then R changes from 0.1 to 0.9 for $\Delta N_1 \simeq N_1 \cot\theta \, \Delta\theta$. If $\theta = 75^{\circ}$ and $\Delta\theta = 10$ mrad, $\Delta N_1/N_1 \simeq 0.003$. If $N_1 = 1.8$, then $\Delta N_1 \simeq 0.005$. Thus it would be possible to discriminate between modes with very close velocities.

Another application is for separating two modes of the same order but with polarizations orthogonal to each other (for example the TE_o and TM_o). Because in general N_1 and N_2 are different for these two modes, we can find a θ so that one mode will be reflected while the other will be transmitted. This is equivalent to a nicol prism in three-dimensional optics. This technique may be more useful than the selective absorption method proposed by Rollke and Sohler (Ref. 9), or the polarization filter by Mahlein (Ref. 10). This latter one uses the transmission, at Brewster's angle, of a multilayer structure deposited on a guide. The discrimination is less than 20 dB. Moreover, it does not conserve the TE_o mode in the guide; this may limit its application.

8.0 CONCLUSION

Experimental measurements have demonstrated that the theory of evanescent tunnelling to explain the behavior of a variable guided beam splitter is valid for a physically acceptable waveguide thickness profile. Some difficulties arose in the explanation of the TE_o results, but this was shown to be due to a gross approximation made in the calculation. Since the splitting effect is anyway quite similar for the two families of modes, more accurate calculations were not done. Sheem & Tsai (Ref. 11) have used a similar technique to build a very simple electro-optical switch. But, as the effective index variation is quite abrupt in their device, there are problems associated with geometric match in four port networks (Ref. 12) which do not exist in the small gap ($c/\lambda \simeq 2$) device presented here. The expression (19) in (Ref. 12) corresponds to an approximation of T (given by our eq. 2) at large δ. Such immediate applications as a beam splitter, a polarization analyser and a mode selector have also been discussed. Finally, this device may be scaled to longer wavelengths using appropriate fabrication techniques and materials.

9.0 REFERENCES

1. Vincent, D. and Lit, J.W.Y., "Optique bidimensionnelle en couche mince", Can. J. Phys., Vol. 57, p. 45, 1979.

2. Ingrey, S.J., Westwood, W.D., Cheng, Y.C., and Wei, J., "Variable Refractive Index and Birefringent Waveguides by Sputtering Tantalum in O_2/N_2 Mixtures", Appl. Opt., Vol. 14, p. 2194, 1975.

3. Vincent, D. and Lit, J.W.Y., "Thin-Film Beam Splitter for Integrated Optics", Jour. Opt. Soc. Amer., Vol. 67, p. 533, 1977.

4. Ulrich, R. and Torge, R., "Measurement of Thin-Film Parameters with a Prism Coupler", Appl. Opt., Vol. 12, p. 2901, 1973.

5. Westwood, W.D., "Calculation of Deposition Rates in Diode Sputtering Systems", J. Vac. Sci. Technol., Vol. 15, p. 1, 1978.

6. Abramowitz, M. and Stegun, I.A., Ed. "Handbook of Mathematical Functions", p. 446, Dover, New York, 1972.

7. Ulrich, R., "Theory of the Prism-Film Coupler by Plane Wave Analysis", Jour. Opt. Soc. Amer., Vol. 60, p. 1337, 1970.

8. Tsang, W.T. and Wang, S., "Thin-Film Beam Splitter and Reflector for Optical Guided Waves", Appl. Phys. Lett., Vol. 27, p. 588, 1975.

9. Rollke, K.H. and Sohler, W., "Metal-Clad Waveguide as Cut-Off Polarizer for Integrated Optics", IEEE Trans., Vol. QE-13, p. 141, 1977.

10. Mahlein, H.F., "Integrated Optical Polarizer", Digest Tech. pap., Topical Meeting on Integrated Optics, Salt Lake City, Utah January 1976, Paper MD1.

11. Sheem, S.K. and Tsai, C.S., "Light Beam Switching and Modulation Using a Built-In Dielectric Channel in $LiNbO_3$ Planar Waveguide", Appl. Opt., Vol. 17, p. 892, 1978.

12. Sheem, S.K., "Total Internal Reflection Integrated-Optics Switch: a Theoretical Evaluation", Appl. Opt., Vol. 17, p. 3679, 1978.

CRDV R-4161/79 (NON CLASSIFIE)

Bureau - Recherche et Développement, MDN, Canada.
CRDV, C.P. 880, Courcelette, Qué. G0A 1R0

"Etude expérimentale d'une séparatrice pour un faisceau optique guidé"
par D. Vincent, J.W.Y. Lit, P. Lavigne et G. Otis

Nous avons mesuré la réflectivité R d'une séparatrice pour faisceau optique guidé. La méthode de fabrication, utilisant un fil mince comme masque, donne au guide plan une variation d'épaisseur de forme parabolique. Les résultats expérimentaux indiquent clairement que l'expression théorique $R=\tanh^2\delta$ décrit bien ce phénomène, surtout dans le cas d'un mode TM_0. Nous discutons également de quelques applications possibles de cette structure telles qu'un analyseur de polarisation et un sélecteur de modes. (NC)

CRDV R-4161/79 (NON CLASSIFIE)

Bureau - Recherche et Développement, MDN, Canada.
CRDV, C.P. 880, Courcelette, Qué. G0A 1R0

"Etude expérimentale d'une séparatrice pour un faisceau optique guidé"
par D. Vincent, J.W.Y. Lit, P. Lavigne et G. Otis

Nous avons mesuré la réflectivité R d'une séparatrice pour faisceau optique guidé. La méthode de fabrication, utilisant un fil mince comme masque, donne au guide plan une variation d'épaisseur de forme parabolique. Les résultats expérimentaux indiquent clairement que l'expression théorique $R=\tanh^2\delta$ décrit bien ce phénomène, surtout dans le cas d'un mode TM_0. Nous discutons également de quelques applications possibles de cette structure telles qu'un analyseur de polarisation et un sélecteur de modes. (NC)

CRDV R-4161/79 (NON CLASSIFIE)

Bureau - Recherche et Développement, MDN, Canada.
CRDV, C.P. 880, Courcelette, Qué. G0A 1R0

"Etude expérimentale d'une séparatrice pour un faisceau optique guidé"
par D. Vincent, J.W.Y. Lit, P. Lavigne et G. Otis

Nous avons mesuré la réflectivité R d'une séparatrice pour faisceau optique guidé. La méthode de fabrication, utilisant un fil mince comme masque, donne au guide plan une variation d'épaisseur de forme parabolique. Les résultats expérimentaux indiquent clairement que l'expression théorique $R=\tanh^2\delta$ décrit bien ce phénomène, surtout dans le cas d'un mode TM_0. Nous discutons également de quelques applications possibles de cette structure telles qu'un analyseur de polarisation et un sélecteur de modes. (NC)

CRDV R-4161/79 (NON CLASSIFIE)

Bureau - Recherche et Développement, MDN, Canada.
CRDV, C.P. 880, Courcelette, Qué. G0A 1R0

"Etude expérimentale d'une séparatrice pour un faisceau optique guidé"
par D. Vincent, J.W.Y. Lit, P. Lavigne et G. Otis

Nous avons mesuré la réflectivité R d'une séparatrice pour faisceau optique guidé. La méthode de fabrication, utilisant un fil mince comme masque, donne au guide plan une variation d'épaisseur de forme parabolique. Les résultats expérimentaux indiquent clairement que l'expression théorique $R=\tanh^2\delta$ décrit bien ce phénomène, surtout dans le cas d'un mode TM_0. Nous discutons également de quelques applications possibles de cette structure telles qu'un analyseur de polarisation et un sélecteur de modes. (NC)

DREV R-4161/79 (UNCLASSIFIED)

Research and Development Branch, DND, Canada.
DREV, P.O. Box 880, Courcelette, Que. G0A 1R0

"Experimental Study of an Optical Guided-Beam Splitter"
by D. Vincent, J.W.Y. Lit, P. Lavigne and G. Otis

Measurements on the reflectance R of a guided-beam splitter have been performed. The fabrication method, based on the use of a thin wire as a mask, produces a groove with a parabolic thickness profile in a planar waveguide. The experimental results demonstrate that the theoretical expression $R=\tanh^2\delta$ describes well the observed phenomena, especially when the TM_0 mode is incident on the groove. Additional applications of this device for polarization analysis and mode selection are also discussed. (U)

DREV R-4161/79 (UNCLASSIFIED)

Research and Development Branch, DND, Canada.
DREV, P.O. Box 880, Courcelette, Que. G0A 1R0

"Experimental Study of an Optical Guided-Beam Splitter"
by D. Vincent, J.W.Y. Lit, P. Lavigne and G. Otis

Measurements on the reflectance R of a guided-beam splitter have been performed. The fabrication method, based on the use of a thin wire as a mask, produces a groove with a parabolic thickness profile in a planar waveguide. The experimental results demonstrate that the theoretical expression $R=\tanh^2\delta$ describes well the observed phenomena, especially when the TM_0 mode is incident on the groove. Additional applications of this device for polarization analysis and mode selection are also discussed. (U)

DREV R-4161/79 (UNCLASSIFIED)

Research and Development Branch, DND, Canada.
DREV, P.O. Box 880, Courcelette, Que. G0A 1R0

"Experimental Study of an Optical Guided-Beam Splitter"
by D. Vincent, J.W.Y. Lit, P. Lavigne and G. Otis

Measurements on the reflectance R of a guided-beam splitter have been performed. The fabrication method, based on the use of a thin wire as a mask, produces a groove with a parabolic thickness profile in a planar waveguide. The experimental results demonstrate that the theoretical expression $R=\tanh^2\delta$ describes well the observed phenomena, especially when the TM_0 mode is incident on the groove. Additional applications of this device for polarization analysis and mode selection are also discussed. (U)

DREV R-4161/79 (UNCLASSIFIED)

Research and Development Branch, DND, Canada.
DREV, P.O. Box 880, Courcelette, Que. G0A 1R0

"Experimental Study of an Optical Guided-Beam Splitter"
by D. Vincent, J.W.Y. Lit, P. Lavigne and G. Otis

Measurements on the reflectance R of a guided-beam splitter have been performed. The fabrication method, based on the use of a thin wire as a mask, produces a groove with a parabolic thickness profile in a planar waveguide. The experimental results demonstrate that the theoretical expression $R=\tanh^2\delta$ describes well the observed phenomena, especially when the TM_0 mode is incident on the groove. Additional applications of this device for polarization analysis and mode selection are also discussed. (U)